Assessment of grid-side filters for three-phase current-source inverter PV systems

Thomas Geury[1,2], Sonia Pinto[2], Johan Gyselinck[1]

Abstract – *In this paper, three grid-side filter topologies for grid-connected three-phase photovoltaic current-source inverters are designed and assessed based on the Total Harmonic Distortion (THD) of the grid currents, on the power factor in the connection to the grid, and on the filter losses. A second-order CL filter with passive damping resistors in parallel with the filter inductors is first sized and evaluated. It is then improved by removing the resistors and using active damping, with the virtual resistor method and feedback of the inductor voltages requiring no additional measurements. The analysis is conducted taking into account the delays introduced in the control circuit and the cross-terms in the state-space equations in the synchronous dq frame. A fourth-order CLCL filter is also sized and considered as an alternative grid-side filter topology to reduce the switching harmonics. Simulation and experimental results obtained with a direct control approach confirm the proper sizing and operation of the filters. Based on the THD of the grid currents and filter losses, the second-order filter with active damping presents the best results with a THD lower than 5 % and nearly negligible losses.*

Keywords*: Renewable energy, Power Quality, Current-source inverter, Low-pass filters, High-frequency harmonics*

Nomenclature

Symbol	Description	Units
C	Single-phase equivalent of C_{ac}	F
C_{ac}	Grid-side filter capacitance	F
C_1, C_2	Fourth-order filter capacitances	F
c_D, c_Q	Sliding mode control variables	
DPF	Displacement power factor ($cos\ \phi$)	–
f_0	Grid-side filter resonance frequency	Hz
f_c	Grid-side filter cutoff frequency	Hz
f_g	Grid frequency	Hz
f_{sw}	CSI switching frequency	Hz
$G(s)$	CSI transfer function	–
$H(s)$	Virtual resistor transfer function	A/V
i	Grid current	A
i_a	Line current of phase a	A
i_c	Grid-side filter capacitor current	A
I_{dc}	dc link current	A
i_ℓ	Grid-side filter inductor current	A
i_s	CSI ac current	A
I_{SC}	PV array short-circuit current	A
$K(s)$	Active damping feedback transfer function	–
k_1	Grid-side filter ripple factor	–
L	Single-phase equivalent of L_{ac}	H
L_{ac}	Grid-side filter inductance	H
L_{dc}	dc link inductance	H
L_1, L_2	Fourth-order filter inductances	H
P_d	Grid-side filter damping losses	W
P_{PV}	PV array nominal power	W
Q_c	Grid-side filter capacitor reactive power	var
R_{db}	Fourth-order filter passband ripple	dB
r_p	Grid-side filter damping resistance	Ω
r_1, r_2	Fourth-order filter damping resistances	Ω
$\mathbf{S}$	Switching matrix of the CSI	–
$S(e_x)$	Sliding surface of the ac variable x	
S_{kj}	CSI switch, $k = \{1,2\}$, $j = \{1,2,3\}$	–
T_d	Time delay introduced by the CSI	s
T_s	Simulation and experiment sample time	s
T_{sw}	CSI switching period	s
v	Grid voltage	V
v_a	Line-to-ground ac voltage of phase a	V
v_ℓ	Grid-side filter inductor voltage	V
V_{OC}	PV array open-circuit voltage	V
V_{PV}	PV array voltage	V
v_s	CSI ac voltage	V
Δx	Ripple of the variable x	
x_{dq}	dq-axis components of the ac variable x, $x_{dq} = \{x_d, x_q\}$	
x_h	Harmonic h of the ac variable x	
x_{max}	Amplitude of the ac variable x	
x_{rms}	rms value of the ac variable x	
$\tilde{X}$	Phasor of the ac variable x	
Z	Fourth-order filter scaling impedance	s/rad
ω_g	Grid pulsation	rad/s
ω_s	CSI switching pulsation ($\omega_s = 2\pi f_s$)	rad/s
ϕ	Phase angle of the grid voltages	rad
ζ	Damping ratio	–

Manuscript received August 2016, revised August 2016

I. Introduction

Over the last years, the penetration of Distributed Generation (DG) in the Medium-Voltage (MV) and, in particular, in the Low-Voltage (LV) grid has increased and is expected to keep increasing in the near future. However, this massive introduction of power electronics-based equipment in the grid will result in additional Power Quality (PQ) issues, namely high-order current harmonics that will increase the distortion of the grid voltages.

International standards [1], [2] such as IEEE 1547 (2003) and IEC 61727 (current Total Harmonic Distortion (THD) < 5 % and Displacement Power Factor (DPF) > 0.9) for Photovoltaic (PV) systems connected to the utility interface have been developed in this perspective. The topology and design of the grid-side filter are important characteristics of the PV system influencing the attenuation of the switching harmonics and the reduction of the THD of the grid currents.

A three-phase PV system using a single-stage Current-Source Inverter (CSI) with an inductor in the dc link to smooth the dc current is considered in this work [3]. The CSI acts as a voltage-step-up converter, such that the converter ac voltages are risen up to the level of the grid voltages without the need for an additional conversion stage or voltage-step-up transformer and with lower PV string voltage compared to the more common Voltage-Source Inverter (VSI) systems [4], [5]. The standard grid-side filter topology for a CSI is a second-order CL filter with passive damping resistors [6], [7]—higher-order grid-side filters may also be used despite the little attention they have received in the literature [6]. The damping resistors are commonly connected in parallel with the filter inductors—other configurations with higher losses have been proposed in the literature [6], [8].

Passive damping has the advantage of not requiring additional measurements. However, it implies extra components with losses and hinders the attenuation of the high-order harmonics. On the contrary, the active damping alternative does not require any resistive components since the damping is achieved by acting on the control of the system. It provides a better attenuation of high-order harmonics, specifically at the switching frequency, together with a better efficiency. On the downside, it increases the complexity of the control system and extra voltage or current sensors are often required [9].

Filter- and multiloop-based active damping methods have been developed in the literature for VSI systems. The former use a higher-order controller with an additional block in the control loop, without requiring extra sensors [10], [11]. However, without a precise knowledge of the system parameters, it is harder to tune the controller parameters. The latter consists in additional control loops and can be implemented either with full-state feedback or a virtual resistor. Full-state feedback requires several extra sensors in the system. Hence, dual-loop feedback with a virtual resistor is commonly the preferred method [8], [11]–[17].

This method consists in using the feedback of one of the filter variables and subtracting it to the converter reference to obtain an effect equivalent to that of a passive damping resistor. The feedback variable is most often the capacitor current [12]–[15] but other variables such as the capacitor voltage or grid-side current [14] and the grid-side or converter-side inductor voltage [8] can be used. In this work, the method is applied on the filter inductor voltages and a feedback of the grid currents is used so that no extra sensor is required.

The delay introduced by the converter is mostly not taken into account when developing the active damping method [11], [14], [16], [17]. This gap has been filled with filter-based damping [10], with virtual resistor capacitor current feedback [12], [13], [15], and with the lead-lag network method [18]. Also, a single-phase circuit [13], [14] or the approximation of an equivalent single-phase system [8], [11], [12] is used in most papers to tune the active damping feedback gain. This is then applied directly to the PWM reference generation [11]–[14] or separately for i_d and i_q [10], neglecting the cross terms in the analysis. The analysis of the *dq*-axis transfer functions can also be conducted [16], which is done in this paper.

In this work we develop a virtual resistor active damping method applied to a second-order grid-side filter for the connection of the less common CSI PV system to the LV grid. The delay introduced by the converter and the delta connection of the filter capacitors are considered for a complete and consistent analysis, as opposed to most of the works on the subject. Also, passively damped second- and fourth-order filters are designed maximising the DPF in the connection to the grid; the latter is an interesting alternative that has received little attention in the literature. The obtained results are compared based on the THD of the grid currents and the filter losses. Experimental results for the second-order filter topology confirm the proper operation of the actively damped system.

II. Second-order filter with passive damping

The three-phase single-stage grid-connected CSI PV system [3] is presented in Fig. 1 and is briefly detailed in the next sections—the system is first considered with passive damping and guarantees a nearly unitary DPF together with the control of the PV array power P_{PV}, using direct sliding mode control. A second-order CL grid-side filter with passive damping is considered as the reference topology to attenuate the CSI switching harmonics [7].

II.1. Dynamic model of the grid-side filter

Ideal grid-voltage sources are considered with

$$v_i = \sqrt{2} v_{\text{rms}} \cos\left(\omega t + \phi - (j-1)\tfrac{2\pi}{3}\right), \quad ij = \{\text{a1,b2,c3}\} \quad (1)$$

with a constant pulsation $\omega = \omega_g$ and reference phase angle ϕ.

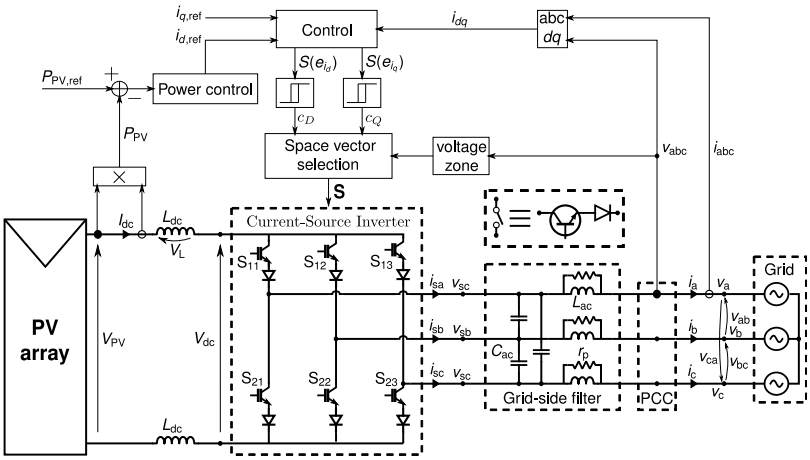

Fig. 1. Three-phase single-stage grid-connected CSI PV system with a passively damped second-order grid-side filter, and its control circuit

To obtain a time-invariant state-space model of the grid-side filter the Concordia-Park transform is used and the state variables in the synchronous *dq* frame are the grid currents i_d and i_q, and the filter input voltages v_{sd} and v_{sq} [3]. Considering the damping resistors r_p in parallel with the grid-side filter inductors, as shown in Fig. 1, the state-space equations are first expressed with the grid-side filter inductor currents $i_{\ell d}$ and $i_{\ell q}$ as state variables:

$$\begin{aligned}
\frac{\mathrm{d}i_{\ell d}}{\mathrm{dt}} &= \omega i_{\ell q} + \frac{1}{2L_\mathrm{ac}} v_{sd} + \frac{1}{2\sqrt{3}L_\mathrm{ac}} v_{sq} - \frac{1}{L_\mathrm{ac}} v_d \\
\frac{\mathrm{d}i_{\ell q}}{\mathrm{dt}} &= -\omega i_{\ell d} - \frac{1}{2\sqrt{3}L_\mathrm{ac}} v_{sd} + \frac{1}{2L_\mathrm{ac}} v_{sq} - \frac{1}{L_\mathrm{ac}} v_q \\
\frac{\mathrm{d}v_{sd}}{\mathrm{dt}} &= \omega v_{sq} - \frac{1}{3C_\mathrm{ac}r_\mathrm{p}} v_{sd} - \frac{1}{2C_\mathrm{ac}} i_{\ell d} + \frac{1}{2\sqrt{3}C_\mathrm{ac}} i_{\ell q} \\
&\quad + \frac{1}{2C_\mathrm{ac}} i_{sd} - \frac{1}{2\sqrt{3}C_\mathrm{ac}} i_{sq} + \frac{1}{2C_\mathrm{ac}r_\mathrm{p}} v_d - \frac{1}{2\sqrt{3}C_\mathrm{ac}r_\mathrm{p}} v_q \\
\frac{\mathrm{d}v_{sq}}{\mathrm{dt}} &= -\omega v_{sd} - \frac{1}{3C_\mathrm{ac}r_\mathrm{p}} v_{sq} - \frac{1}{2\sqrt{3}C_\mathrm{ac}} i_{\ell d} - \frac{1}{2C_\mathrm{ac}} i_{\ell q} \\
&\quad + \frac{1}{2\sqrt{3}C_\mathrm{ac}} i_{sd} - \frac{1}{2C_\mathrm{ac}} i_{sq} + \frac{1}{2\sqrt{3}C_\mathrm{ac}r_\mathrm{p}} v_d + \frac{1}{2C_\mathrm{ac}r_\mathrm{p}} v_q
\end{aligned} \tag{2}$$

where the CSI ac currents i_{sd} and i_{sq}, and the grid voltages v_d and v_q are independent variables. The grid currents can then be obtained with

$$\begin{aligned}
i_d &= i_{\ell d} + \frac{1}{2r_\mathrm{p}} v_{sd} + \frac{1}{2\sqrt{3}r_\mathrm{p}} v_{sq} - \frac{1}{r_\mathrm{p}} v_d \\
i_q &= i_{\ell q} - \frac{1}{2\sqrt{3}r_\mathrm{p}} v_{sd} + \frac{1}{2r_\mathrm{p}} v_{sq} - \frac{1}{r_\mathrm{p}} v_q
\end{aligned} \tag{3}$$

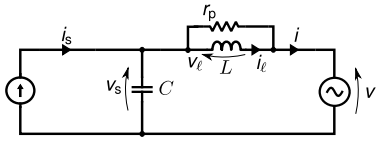

Fig. 2. Single-phase equivalent scheme of the second-order filter with passive damping

II.2. Sizing of the filter components

The single-phase equivalent of the second-order filter with passive damping and processing only one third of the total power is shown in Fig. 2, where $L = L_\mathrm{ac}$ and $C = 3C_\mathrm{ac}$ are used for simpler notations. The filter transfer function is

$$\frac{i(s)}{i_\mathrm{s}(s)} = \frac{s\,L/r_\mathrm{p} + 1}{s^2 LC + s\,L/r_\mathrm{p} + 1}\,. \tag{4}$$

The sizing of the filter components depends on several conditions and requirements [7], [9], [19]:

1. Maximisation of the DPF at the grid frequency by sizing the capacitors so that the grid voltage and current phase-shift is negligible or easily compensated by the grid current controller. Considering a reactive power consumption Q_c in the filter capacitor and a rated PV array power P_PV, the DPF reads

$$\mathrm{DPF} = \frac{P_\mathrm{PV}}{\sqrt{P_\mathrm{PV}^2 + Q_\mathrm{c}^2}}\,, \tag{5}$$

without taking the system efficiency into account. The DPF is here considered instead of the power factor ($\mathrm{PF} = P_\mathrm{PV} \big/ \left(P_\mathrm{PV}^2 + Q_\mathrm{c}^2 + D^2\right)$, where D is the distortion power dependent on high-order harmonics), to focus on the phase-shift between current and voltage fundamental components rather than their harmonic distortion. Using only the voltage and current fundamental components, the reactive power associated to the filter capacitor is:

$$Q_\mathrm{c} = v_{\mathrm{s},1}^2 \omega_\mathrm{g} C\,, \tag{6}$$

where $\omega_\mathrm{g} = 2\pi f_\mathrm{g}$ is the grid pulsation and the fundamental component of the capacitor voltage $v_{\mathrm{s},1}$ can be expressed in function of the grid and inductor voltages, without considering the damping resistors and system losses: $\tilde{V}_{\mathrm{s},1} = \tilde{V} + j\omega_\mathrm{g} L P_\mathrm{PV} / 3v$. The voltage drop in the inductor can be neglected at the grid frequency, such that $v_{\mathrm{s},1} \simeq v$ and, using (5) and (6), the resulting condition on the single-phase equivalent capacitance is

$$C < \frac{P_{\mathrm{PV}}}{\omega_{\mathrm{g}} v^2} \sqrt{\frac{1}{\mathrm{DPF}^2} - 1} \,. \tag{7}$$

2. Minimisation of the THD of the grid current by reducing its high-frequency ripple which can be expressed as a fraction of the fundamental component:

$$\Delta i_{\max} = k_1 i_{1,\mathrm{rms}} \,. \tag{8}$$

The capacitor voltage can be estimated from $v_{\mathrm{s}} = v_{\mathrm{s},1} + \Delta v_{\mathrm{s}}$, with $v_{\mathrm{s},1}$ the fundamental component and Δv_{s} the ripple. From Fig. 2, the current in the filter inductor is $i_\ell = \frac{1}{L}\int \left(v - v_{\mathrm{s}}\right) \mathrm{d}t$. Considering a nearly ideal grid voltage we have

$$i_\ell = \frac{1}{L}\int \left(v - v_{\mathrm{s},1}\right) \mathrm{d}t + \frac{1}{L}\int \left(-\Delta v_{\mathrm{s}}\right) \mathrm{d}t \,, \tag{9}$$

and the ripple of the inductor current may be estimated solving $\Delta i_\ell = \frac{1}{L}\int \left(-\Delta v_{\mathrm{s}}\right) \mathrm{d}t$. Assuming that Δv_{s} is a nearly triangular waveform, the rms value of the inductor current ripple is $\Delta i_{\ell,\mathrm{rms}} = 2\Delta i_{\max} / \sqrt{30}$. Without considering the damping resistor, the total rms value of the grid current is approximated with

$$i_{\mathrm{rms}} \simeq \sqrt{i_{1,\mathrm{rms}}^2 + \left(2\Delta i_{\max} / \sqrt{30}\right)^2} \,, \tag{10}$$

and the THD of the current is computed with

$$\mathrm{THD_i} \simeq \frac{2k_1}{\sqrt{30}} \,. \tag{11}$$

The condition on the inductance is first expressed as a function of the ripple amplitude:

$$L > \frac{I_{\mathrm{dc}}}{32C\ f_{\mathrm{sw}}^2 \Delta i_{\max}} \,, \tag{12}$$

where I_{dc} is the rated dc link current. Using the expression of the THD in (11) and the relation in (8), we finally have

$$L > \frac{I_{\mathrm{dc}}}{16\sqrt{30} C f_{\mathrm{sw}}^2 \mathrm{THD_i} i_{1,\mathrm{rms}}} \,. \tag{13}$$

3. Adjustment of the resonance frequency $f_0 = 1/\left(2\pi\sqrt{LC}\right)$ to be nearly a decade lower than the switching frequency and at least a decade higher than the grid frequency. The cutoff frequency is such that the switching harmonics are attenuated while avoiding resonance issues and allowing for low-order harmonics compensation if active filtering is used.

Assuming the ratings in Table I with a PV array power of 1.5 kW and a nominal dc link current of 10.5 A, the filter is sized according to the above conditions:

TABLE I.
PARAMETER VALUES (SECOND-ORDER FILTER)

Symbol	Description	Value	Units
f_{sw}	Switching frequency[a]	5	kHz
v	Grid phase rms voltage	120	V
f_{g}	Grid frequency	50	Hz
P_{PV}	PV array nominal power	1.5	kW
V_{OC}	PV array OC voltage	180.5	V
I_{SC}	PV array SC current	11.78	A
L_{dc}	dc link inductance	12	mH
C_{ac}	Grid-side filter capacitance (Δ)	10	μF
L_{ac}	Grid-side filter inductance	3	mH
r_{p}	Damping resistance	48	Ω

[a]The value is variable and may be a bit lower due to the sliding mode control approach employed here [3].

1. The reactive power limit is considered as a decrease of 5 % of the DPF at rated power [19]. The resulting condition is C < 35.37 μF and a value of 30 μF is chosen for convenience of implementation. The three-phase capacitance is divided by 3 to consider the three-phase delta connection: C_{ac} = 10 μF.
2. A THD of 3 % is considered to guarantee that the 5 % limit is met [1], [2] even in non-ideal conditions or with the use of passive damping. The resulting inductance is $L \simeq$ 3 mH, with a ripple factor of k_1 = 0.08.
3. The resonance frequency results in f_0 = 530.5 Hz and is in a range around 500 Hz to meet the above condition.

II.3. Sizing of the damping resistors

Passive damping is applied by placing the damping resistors in parallel with the filter inductors [6], [7], [20]. The slope of the magnitude Bode plot of the transfer function (4) goes from -40 dB/decade (2 poles) to -20 dB/decade (2 poles and 1 zero) when adding the damping resistor, which clearly decreases the attenuation of the high-order harmonics. In order to minimise this effect and still have a good attenuation of the switching harmonics, the zero $s = r_{\mathrm{p}}/L$ should be located at a frequency around the switching frequency f_{sw} [21]. Thus, we have $r_{\mathrm{p}} \simeq 2\pi f_{\mathrm{sw}} L$ = 94.25 Ω, considering a switching frequency of 5 kHz. However, a trade-off must be found in order to guarantee a good damping of the system [20], based on the damping ratio

$$\zeta = \frac{1}{2 r_{\mathrm{p}} C \omega_0} \,. \tag{14}$$

TABLE II.
COMPARISON OF FILTER CHARACTERISTICS FOR DIFFERENT PASSIVE DAMPING RESISTANCES

r_{p} [Ω]	Losses [W]	Attenuation at f_{sw} [dB]	Damping ratio (ζ)
10	5.07	-19.5	0.58
25	2.89	-27	0.23
48	2.66	-32	0.12

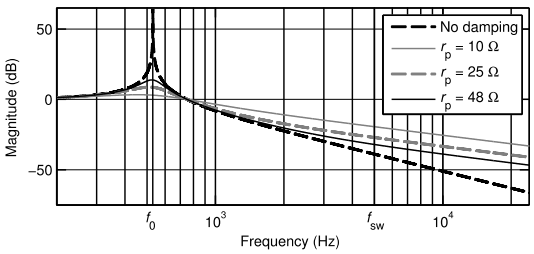

Fig. 3. Magnitude Bode plots of the single-phase equivalent transfer function between i (s) and i_s (s) of the grid-side filter with different passive damping resistances

Thus, a high damping resistance decreases the stability and the effectiveness of the damping of the oscillations. The losses in the damping resistors should be limited to approximately 0.3 % of the nominal power [6], i.e. 4.5 W in this case. These can be computed with

$$P_\mathrm{d} = 3\frac{\sum_h v_{\ell,h}^2}{r_\mathrm{p}}, \tag{15}$$

where all the harmonics of the inductor voltage are considered with $\tilde{V}_{\ell,h} = X_{\ell,h}\tilde{I}_h = jr_\mathrm{p}h\omega_\mathrm{g}L\big/\left(r_\mathrm{p} + jh\omega_\mathrm{g}L\right)\tilde{I}_h$ [19], [21]. The approximation in (10) is used, considering two components of the grid currents: the fundamental ($h = 1$) and an approximation of the other harmonics around the switching frequency ($h \simeq h_\mathrm{s}$). The total losses can thus be obtained with

$$P_\mathrm{d} = P_{\mathrm{d},1} + P_{\mathrm{d},hs}. \tag{16}$$

The losses related to the fundamental component are

$$P_{\mathrm{d},1} = 3\frac{v_{\ell,1}^2}{r_\mathrm{p}} = 3\frac{\omega_\mathrm{g}^2 L^2}{r_\mathrm{p}} i_{1,\mathrm{rms}}^2, \tag{17}$$

where the term $h\omega_\mathrm{g}L$ is negligible in relation to r_p at the grid frequency [21]. Based on (10), the losses related to the harmonic components of the grid currents are obtained:

$$P_{\mathrm{d},hs} = 3\frac{r_\mathrm{p}\omega_\mathrm{s}^2 L^2}{r_\mathrm{p}^2 + \omega_\mathrm{s}^2 L^2}\left(\frac{2\Delta i_\mathrm{max}}{\sqrt{30}}\right)^2, \tag{18}$$

where $\omega_\mathrm{s} = 2\pi f_\mathrm{sw}$. Expressing the ripple in function of the fundamental component of the grid currents (8), the total damping losses result in

$$P_\mathrm{d} = \frac{\omega_\mathrm{g}^2 L^2}{5r_\mathrm{p}}\left(15 + \frac{2\left(k_1 r_\mathrm{p} h_\mathrm{s}\right)^2}{r_\mathrm{p}^2 + \omega_\mathrm{s}^2 L^2}\right) i_{1,\mathrm{rms}}^2. \tag{19}$$

The damping resistance can be chosen based on the above considerations, the harmonics attenuation at the switching frequency and the damping ratio. These parameters are listed in Table II for different damping resistances and the magnitude Bode plots of the related transfer functions are shown in Fig. 3. A damping resistance of 48 Ω maintains a good attenuation of the switching harmonics, fits the limit of 4.5 W set for the losses and stabilises the system with a damping ratio of 0.12, similar to values of 0.1 [20] and 0.17 [22] used in the literature.

III. Second-order filter with active damping

The single-phase equivalent of the second-order filter with active damping is used (see Fig. 2 without r_p), with the virtual resistor method and a feedback of the inductor voltage. The single-phase equivalent control circuits in Fig. 4 are analysed, leading to the transfer functions of the system and tuning of the active damping gain. The system is then validated with the Bode plots and root loci of the complete analysis in the *dq* frame.

III.1. Single-phase equivalent control circuits

The single-phase equivalent block diagrams of the second-order system without damping, with passive damping and with active damping are represented in Fig. 4. The delay introduced by the converter is modeled by the transfer function

$$G(s) = \frac{i_\mathrm{s}(s)}{i_{\mathrm{s,ref}}(s)} \simeq \frac{1}{T_\mathrm{d}s + 1}, \tag{20}$$

where $T_\mathrm{d} = T_\mathrm{sw}/2$ is the average delay introduced by the converter between a control action on $i_{\mathrm{s,ref}}(s)$ and $i_\mathrm{s}(s)$ [13], [23]. In Fig. 4(c), the active damping is obtained with a feedback of the inductor voltage, using a virtual resistor transfer function H (s) that virtually reproduces the effect of the damping resistor.

The transfer functions of the system are obtained with active and passive damping. With passive damping, neglecting the independent term v considered as a

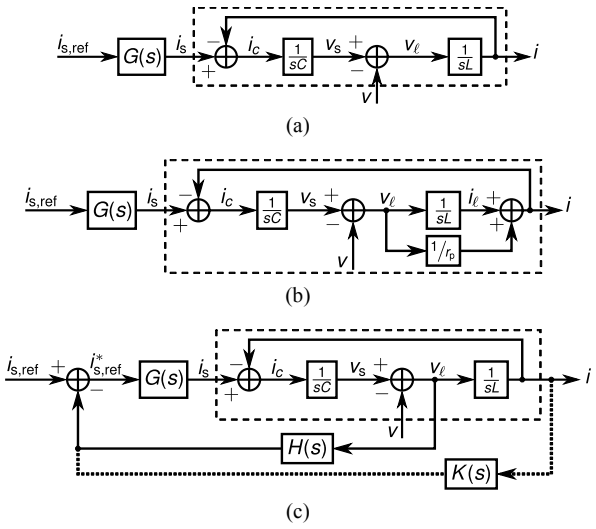

Fig. 4. Block diagram of the single-phase equivalent system with: (a) No damping. (b) Passive damping (resistor r_p). (c) Active damping (feedback of either the inductor voltage with full line or the grid current with dotted line)

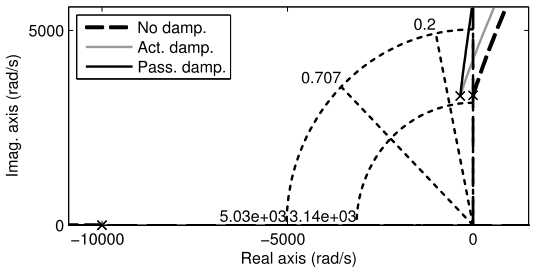

Fig. 5. Root loci of the single-phase equivalent transfer functions without damping, with active damping ($H(s) = 0.021 + 2.08\text{x}10^{-6}s$) and with passive damping ($r_p = 48\ \Omega$)

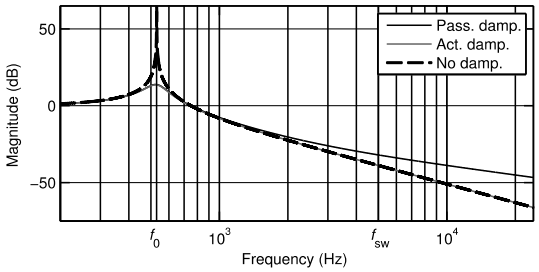

Fig. 6. Magnitude Bode plots of the single-phase equivalent transfer functions between $i(s)$ and $i_{ref}(s)$ for the three second-order filter damping scenarios

perturbation to the system, the transfer function is

$$\frac{i(s)}{i_{s,ref}(s)} = \frac{G(s)\left(1 + sL/r_p\right)}{s^2LC + sL/r_p + 1}. \quad (21)$$

With active damping, the virtual resistor method is used with feedback of the grid-side filter inductor voltage (see full line in Fig. 4(c)). In order to avoid extra measurements, the voltage is obtained from the grid current (see dotted line in Fig. 4(c)) which is already measured for the control of the system: $v_\ell = sLi$. This results in an active damping feedback transfer function

$$K(s) = H(s)sL, \quad (22)$$

and the system transfer function is

$$\frac{i(s)}{i_{s,ref}(s)} = \frac{G(s)}{s^2LC + sLH(s)G(s) + 1}. \quad (23)$$

The virtual resistor transfer function $H(s)$ should be tuned in order to match the effect of the actual damping resistor [11], [24], [25], which, when comparing the denominators of (21) and (23), results in

$$H(s) = \frac{1}{r_p} + \frac{T_d}{r_p}s. \quad (24)$$

The system transfer function with active damping has the advantage of having no zero, which increases the attenuation of high frequencies. Considering a damping resistance of 48 Ω and the parameters in Table I, the virtual resistor transfer function is $H(s) = 0.021 + 2.1\text{x}10^{-6}s$ [A/V] and, from (22), the active damping feedback transfer function on the grid currents is

$$K(s) = 6.25\text{x}10^{-5}s + 6.25\text{x}10^{-9}s^2. \quad (25)$$

The root loci of the single-phase equivalent open-loop system transfer functions without damping, with passive damping and with active damping are shown in Fig. 5, only considering the positive imaginary part for symmetry reasons. The root loci are drawn in function of the controller gain of the grid currents. Limits are drawn for resonance frequencies of 500 Hz or $3.14\text{x}10^3$ rad/s and 800 Hz or $5.03\text{x}10^3$ rad/s (dotted circle arcs), corresponding to cutoff frequencies of 637 Hz and 1 kHz, respectively, and damping ratios of $\sqrt{2}/2$ (0.707) and 0.2 (dotted radial lines). Without damping, the system is unstable as the pairs of complex conjugate closed-loop poles are located in the right half-plane. With passive damping, the system is stable and the damping ratio corresponds to the value computed in Table II. Lower passive damping resistances result in a shift of the closed-loop poles to the left, and thus a better stability of the system, but also a lower attenuation of the switching harmonics, as concluded in the previous section. The use of active damping shifts the open-loop poles into the left half-plane for reproducing the passive damping situation. If the terms of the feedback transfer function are too low, the closed-loop poles are still likely to be located in the right half-plane and the damping ratio is too low. If the gain is too high, then the cutoff frequency increases and the switching harmonics mitigation loses effectiveness.

The magnitude Bode plots for the same damping situations are shown in Fig. 6. Both passive and active damping clearly damp the response at the resonance frequency. However, the high-frequency slope with active damping remains at -40 dB/decade due to the absence of zero in the transfer function, which guarantees a better attenuation of these harmonics when compared to passive damping where the slope is reduced to -20 dB/decade.

III.2. Analysis of the circuit in the dq frame

The complete analysis of the three-phase system is carried out in order to confirm the validity of the active-damping feedback gain computed hereabove.

1) Transfer functions: The three-phase system with delta-connected capacitors is considered without passive damping resistors. It is a particular case of the state-space equations (2), where the damping resistance is infinite [3].

The complete set of transfer functions between the filter input and output currents $i_{sd}(s)$ and $i_{sq}(s)$, and $i_d(s)$ and $i_q(s)$, respectively, is obtained from this model: there are four transfer functions $\text{TF}_{snm}(s) = i_m(s)/i_{sn}(s)$, $n,m = \{d,q\}$. Instead of considering the filter input current or converter ac current $i_s(s)$, the reference of that current $i_{s,ref}(s)$ can be considered by taking the converter delay into account: $\text{TF}_{nm}(s) = \text{TF}_{snm}(s)G(s)$.

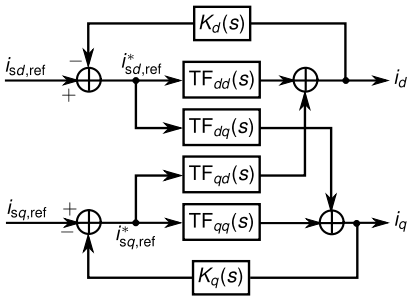

Fig. 7. Schematic representation of active damping and its feedbacks with the set of transfer functions without damping

When using active damping, the feedback needs to be considered in the system transfer functions as it modifies the converter ac current references $i_{sd,\mathrm{ref}}(s)$ and $i_{sq,\mathrm{ref}}(s)$. A scheme of the system with separate feedbacks for *d*- and *q*-axis components is shown in Fig. 7: the transfer functions obtained are used between the modified converter ac current references $i^*_{sdq,\mathrm{ref}}(s)$ and the grid currents $i_{dq}(s)$. Then, the active damping feedback is considered such that the resultant transfer functions $\mathrm{TF_{ad}}$ (s) relating the converter ac current references $i_{sdq,\mathrm{ref}}(s)$ to the grid currents $i_{dq}(s)$ become:

$$\mathrm{TF}_{\mathrm{ad},nn}(s)=\frac{i_n(s)}{i_{sn,\mathrm{ref}}(s)}=\frac{\mathrm{TF}_{nn}(s)}{1+K_n(s)\mathrm{TF}_{nn}(s)},\ n=\{d,q\}$$

$$\mathrm{TF}_{\mathrm{ad},nm}(s)=\frac{i_m(s)}{i_{sn,\mathrm{ref}}(s)},\qquad n,m=\{d,q\},n\neq m \quad (26)$$

$$=\mathrm{TF}_{nm}(s)\left(1-\frac{K_n(s)\mathrm{TF}_{nn}(s)}{1+K_n(s)\mathrm{TF}_{nn}(s)}\right)$$

As mentioned earlier, the feedback is applied to the grid currents to avoid extra measurements. The inductor voltage used for feedback is obtained with $v_{\ell dq}=s\,L_{\mathrm{ac}}\,i_{dq}$, neglecting the cross terms. Considering the virtual resistor transfer functions $H_{dq}(s)$, the feedback transfer functions of the grid currents are:

$$K_{dq}(s)=H_{dq}(s)sL_{\mathrm{ac}}\,. \quad (27)$$

2) Bode plots: The validity of the single-phase equivalent model used to tune the feedback gains is evaluated using the magnitude Bode plots of these sets of system transfer functions with active damping feedback transfer functions $K_{dq}(s)=6.25\mathrm{x}10^{-5}s+6.25\mathrm{x}10^{-9}s^2$ equal to the one in (25).

The magnitude Bode plots of the set of transfer functions are shown in Fig. 8 for the different damping configurations: without damping, with active damping and with passive damping. The plots are the same for the *dd* and *qq* transfer functions, and for the *dq* and *qd* ones. Fig. 8(a) confirms the observations made from the single-phase equivalent transfer functions in Fig. 5 and Fig. 6: there are resonant peaks without damping; passive damping properly attenuates these peaks but the slope of the transfer function in the magnitude plot at high frequencies is slightly

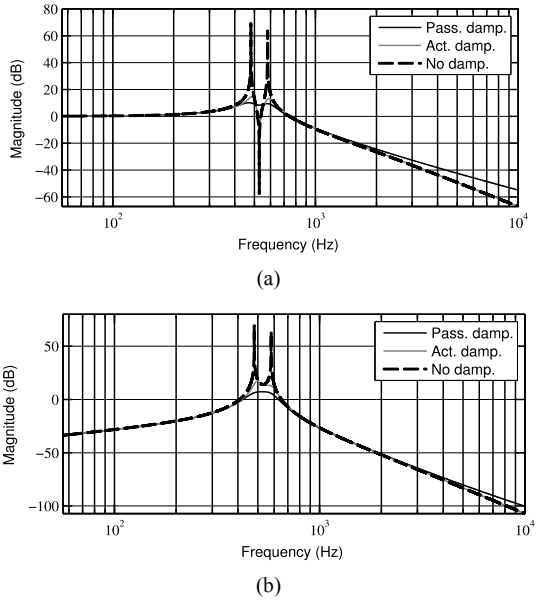

Fig. 8. Magnitude Bode plots of the set of transfer functions in *dq* components, with no damping, with active damping ($H_{dq}(s)=0.021+2.1\mathrm{x}10^{-6}s$ [A/V]) and with passive damping ($r_{\mathrm{p}}=48\ \Omega$): (a) *dd* and *qq* components. (b) *dq* and *qd* components

attenuated which hinders the mitigation of the switching harmonics; with active damping, the high frequencies are properly attenuated but lower frequencies are also attenuated for higher feedback transfer function terms, which are thus to be avoided. Fig. 8(b) shows that the cross terms in the *dq* frame are strongly attenuated, except around the resonance frequency. This confirms the consistency of the single-phase equivalent tuning without cross terms.

IV. Fourth-order filter

A fourth-order CLCL grid-side filter topology, whose single-phase equivalent is presented in Fig. 9, is sized and compared with the previous second-order filter topologies.

IV.1. Components sizing

The CLCL filter considered can be seen as a Chebyshev filter and designed as such [26]. The filter is sized in the single-phase equivalent neglecting the damping resistors, with an order $n=4$.

The sizing of the components depends on three parameters: the cutoff frequency (f_{c}), the passband ripple expressed in dB (R_{db}) and the scaling impedance (Z). The cutoff frequency should be significantly lower than the

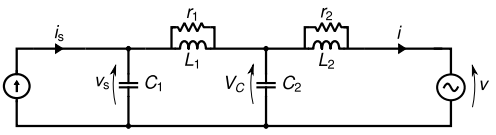

Fig. 9. Single-phase equivalent scheme of the fourth-order filter with passive damping

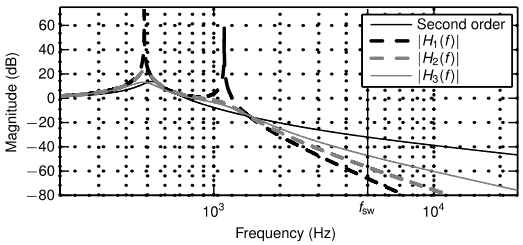

Fig. 10. Magnitude Bode plot of the single-phase equivalent transfer functions between i (s) and i_s (s) of the passively damped second-order filter, and the fourth-order filter without damping resistor (H_1 (s)), and with either one (H_2 (s)) or two of them (H_3 (s))

switching frequency in order to attenuate the switching harmonics; also, it should be well above the grid frequency to avoid any resonance phenomenon: $f_g \ll f_0 \ll f_{sw}$ [26]. The passband ripple is usually chosen around 1 dB or lower and the scaling impedance should be close to the load and source impedances. Also, practical constraints should be considered: the fourth-order filter is expected to reduce the size of the components compared to the second-order filter. In particular, the impedances are inversely proportional to the cutoff frequency.

The above parameters are e.g. chosen as follows: f_c = 1.1 kHz, R_{db} = 1 dB and Z = 20 Ω, which results in C_1 = 5.07 µF, L_1 = 3.1 mH, C_2 = 6.85 µF and L_2 = 2.3 mH. The decrease of the DPF in the connection to the grid is estimated at 5 %, which is within the common limits [19].

IV.2. Transfer functions

The CLCL filter topology is analysed without damping resistors, and with either one or two damping resistors [6]. The performances of these filters are compared.

If no damping resistor is used (r_1, $r_2 \to \infty$), the transfer function between i_s (s) and i (s) reads:

$$H_1(s) = \frac{1}{C_1C_2L_1L_2s^4 + \left(L_2\left(C_1 + C_2\right) + L_1C_1\right)s^2 + 1}, \quad (28)$$

where there are two pairs of complex conjugate poles and no zero. The magnitude Bode plot of this transfer function is shown in Fig. 10; it has two resonance frequencies: one near 500 Hz and the other slightly higher than 1 kHz. Considering one damping resistor r_1, a zero is introduced in the transfer function H_2 (s) and the resonance at 1.1 kHz is damped. With both damping resistors, H_3 (s) has two zeros and the second resonance is damped as well.

As done with the second-order filter, the damping resistances are tuned based on the attenuation at the switching frequency and the losses, using relatively low values that guarantee the stability of the system [6]. Resistances of r_1 = 35 Ω and r_2 = 25 Ω minimise the losses to 2.53 W, which meets the design requirement of 0.3 % of the nominal power [6], considering two cascaded second-order filters. The switching harmonics are attenuated with a gain of -48 dB at the switching frequency. Also, the transfer functions have different slopes for high frequencies: -20 dB/decade for the second-order filter (2 poles and 1 zero), -80 dB/decade for H_1(s) (4 poles), -60 dB/decade for H_2 (s) (4 poles and 1 zero), and -40 dB/decade for H_3 (s) (4 poles and 2 zeros). The fourth-order filter attenuates better the high frequencies compared to the second-order filter with passive damping but the cutoff frequency is higher due to the two resonance peaks.

Even though the fourth-order filter is expected to provide good high-frequency attenuation, it has the drawback of requiring three extra measurements [27]: the inductor current i_ℓ, the capacitor voltage v_s and the non-linear load currents in case advanced non-linear control methods are used to compensate the DPF introduced by the filter [3], [22]. Instead, higher-order linear controllers might be necessary to guarantee a nearly unitary DPF in the connection to the grid [22]. Moreover, with regard to the values obtained for the fourth-order filter, no reduction in weight or volume is expected compared to the second-order filter, as only the capacitances are slightly lowered.

V. Results

The three-phase PV system in Fig. 1 is first studied numerically and then implemented in the laboratory using the parameter values in Table I and the ratings in Table III, with the PV array modeled using the Single Exponential Model (SEM) of a solar cell. The results are all taken at Maximum Power Point (MPP), with $V_{MPP} \simeq$ 83.5 V and $I_{MPP} \simeq$ 6 A, for a rated PV array power of 500 W.

V.1. Simulation results

The system is simulated in the MATLAB/Simulink environment for the three filter configurations under consideration and the results for the grid currents are presented in Fig. 11.

The grid currents with a passively damped second-order filter are shown in Fig. 11(a) and Fig. 11(b) for damping resistances of 25 Ω and 48 Ω, respectively. The latter provides a better attenuation of the switching harmonics with a THD of 4.46 %, which confirms the results from Table II. The THD of the grid currents with active damping, in Fig. 11(c), is reduced to 2.72 %.

Considering the fourth-order filter parameters computed in Section IV.1 and using sliding mode control based on the general theory presented in [23] and [27] for second- and fourth-order systems, respectively, the grid currents are

TABLE III.
SIMULATION AND LABORATORY RATINGS

Symbol	Description	Value	Units
T_s	Sample time	14	µs
v_{rms}	Grid line-to-ground rms voltage	120	V
f_g	Grid frequency	50	Hz
P_{PV}	PV array nominal power	500	W
V_{OC}	PV array OC voltage	105	V
I_{SC}	PV array SC current	6.7	A

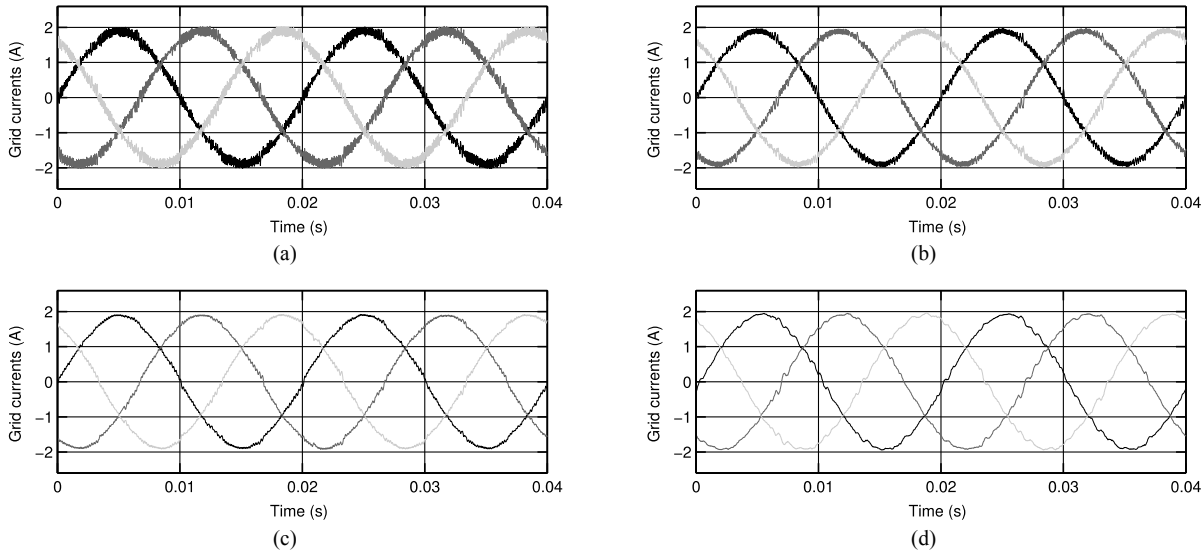

Fig. 11. Simulation grid currents: (a) Passive damping (25 Ω) – THD = 6.74 %. (b) Passive damping (48 Ω) – THD = 4.46 %. (d) Active damping – THD = 2.72 %. (d) Fourth-order filter – THD = 3.20 %

shown in Fig. 11(d) with a THD of 3.20 %. The fourth-order filter does not improve the results compared to the second-order filter with active damping in addition to requiring additional measurements that may lead to stability problems for practical implementation. For these reasons, it has not been considered for experimental results.

V.2. Experimental results

The experiments are performed using the laboratory setup in Fig. 12, with the fast-prototyping software and hardware dSPACE ds1103 (9) and its ControlDesk interface (a). An isolation transformer (8) is added in the connection to the grid (5) and a PV array emulator (1)—max. 1500 W, 360 V and 15 A—is used to supply the CSI module (3), which has the grid-side filter capacitors included (4). The dc link inductors (2), low-dc-voltage supply (6) and measurement board are shown as well.

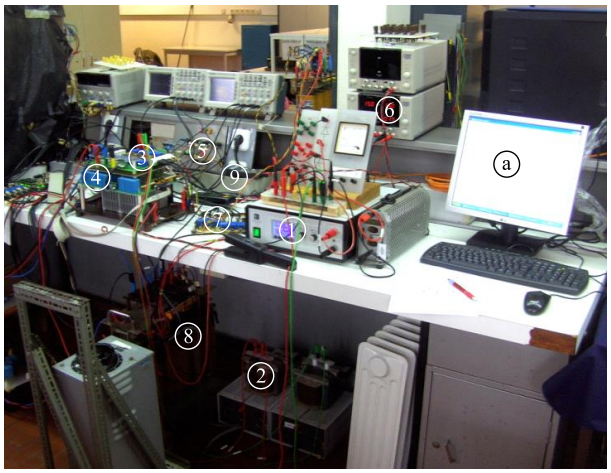

Fig. 12. Experimental setup: (1) PV array emulator, (2) dc link inductors, (3) CSI module, (4) filter capacitors, (5) LV grid, (6) dc power supply, (7) measurement board, (8) isolation transformer, (9) dSPACE board, (a) ControlDesk interface

The results in Fig. 13 confirm that the attenuation of the switching harmonics with passive damping is improved when increasing the damping resistance. In particular, the THD of the grid currents for harmonics up to an order >700 (35 kHz) goes down from 12.70 % to 8.84 % when increasing the resistance from 25 Ω to 48 Ω. With active damping, the grid currents waveforms in Fig. 13(d) present a THD of 4.85 %, which confirms that active damping improves the switching harmonics attenuation.

V.3. Discussion

Three grid-side filter topologies have been designed and tested numerically: a second-order filter with passive/active damping and a fourth-order filter. The results are gathered in Table IV with the different THD values.

The second-order filter with passive damping shows the poorest results regarding the attenuation of the switching harmonics, as expected from the theoretical analyses, even though a damping resistance of 48 Ω results in a THD (simulation) or THD_{40} (experiments) lower than 5 %. In simulation, the actively damped second-order filter results in a THD for the grid currents close to the 2.5 % value used for sizing the filter (see Section II.2).

TABLE IV.
COMPARISON OF THE GRID CURRENTS THD [%] AND EUROPEAN AND FULL-LOAD EFFICIENCIES [%] FOR A SECOND-ORDER FILTER WITH PASSIVE DAMPING (25 Ω – **R25**; 48 Ω – **R48**) AND ACTIVE DAMPING (**AD**)

	Simulation		Laboratory		η_{EU}	η_n
	THD	THD_{40}	THD	THD_{40}		
r25	6.74	2.15	12.70	4.23	95.78	93.23
r48	4.46	1.65	8.84	4.15	95.80	93.26
ad	2.42	2.14	4.85	3.82	95.83	93.31

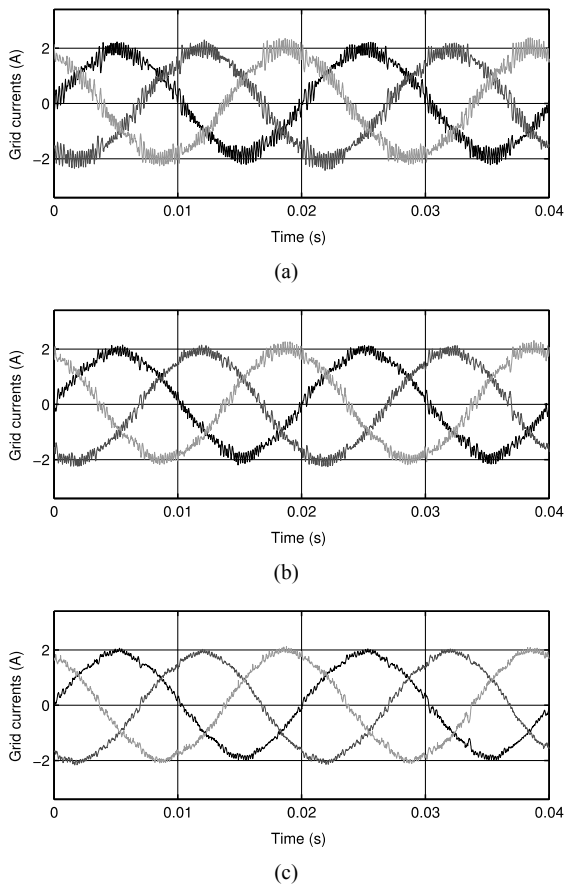

Fig. 13. Experimental grid currents (second-order filter): (a) Passive damping (25 Ω) – THD = 12.70 %, THD_{40} = 4.23 %. (b) Passive damping (48 Ω) – THD = 8.84 %, THD_{40} = 4.15 %. (c) Active damping – THD = 4.85 %, THD_{40} = 3.82 %

The preferred second-order filter with active damping works effectively in the laboratory, as shown by the results in Table IV, where it reduces the THD values of the grid currents compared to the passively damped second-order filter. The THD_{40} of the grid currents for the different experiments is lower than the fixed limit of 5 %, but the switching harmonics are problematic when passive damping is used. The use of active damping allows reducing the THD to 4.85 %, meeting the standards in force, even considering current harmonics up to 35 kHz (h = 700) as opposed to a regular PQ analyser (2 kHz, h = 40).

The European efficiency η_{EU} [2] of the complete CSI system is also shown in Table IV for the second-order filter topologies. As expected, active damping slightly improves the efficiency and results in η_{EU} = 95.82 %, even though the amplitude modulation index is not optimised in that regard. The efficiency at full load η_n is increased from 93.26 % to 93.31 % by using active damping, which confirms that the 0.3 % limit set for the passive damping losses is met.

VI. Conclusion

In this paper grid-side filter topologies for a particular CSI PV system are proposed and sized in order to mitigate the effect of switching harmonics in the grid currents, reducing their THD. Passively damped second- and fourth-order filters have been sized using resistors to mitigate the resonance at the cutoff frequency. To remove the zero introduced by the damping resistor and guarantee a better mitigation of high-order harmonics, the virtual resistor method has been used for active damping, considering the single-phase equivalent circuit of the system. A complete analysis taking into account the converter delay and the *dq*-axis cross terms confirmed the validity of that approach. The fourth-order filter has been sized and the obtained results have been compared with the second-order filter ones. The second-order filter with active damping was considered as the most appropriate method and was implemented in the laboratory in order to confirm the attenuation of the high-order harmonics when compared to the passive damping solution with different damping resistances; the fourth-order filter has not been assessed in the laboratory due to the additional measurements required, the lower stability, and the absence of reduction in volume and weight. Active damping guarantees that the grid currents meet the standards in force with a resulting THD of 4.85 %, even considering harmonics higher than h = 40.

Acknowledgements

This research project was funded by the Belgian Fund for training in Research in Industry and in Agriculture (F.R.I.A.). This work was also supported by the national funds through Fundação para a Ciência e Tecnologia (FCT) with reference UID/CEC/50021/2013.

References

[1] B. Singh, A. Chandra, K. Al-Haddad, *Power Quality Problems and Mitigation Techniques*, First edit. (John Wiley and Sons Ltd, 2015).

[2] R. Teodorescu, M. Liserre, P. Rodriguez, *Grid converters for photovoltaic and wind power systems* (John Wiley & Sons, Ltd., 2011).

[3] T. Geury, S. Pinto, J. Gyselinck, Current source inverter-based photovoltaic system with enhanced active filtering functionalities, *IET Power Electronics*, *vol. 8 n.* 12, December 2015, pp. 2483–2491.

[4] G. Ertasgin, W. L. Soong, N. Ertugrul, Analysis and Design of Single-Phase Current-Source Grid-Connected PV Inverter, *The 15th European Conference on Power Electronics and Applications, EPE'13 ECCE Europe*, September 3-5, 2013, Lille, France.

[5] R. Uthirasamy, U. S. Ragupathy, V. Kumar Chinnaiyan, C. Megha, Experimentation of Boost Chopper Interfaced Cascaded Multilevel Inverter Topology for Photovoltaic Applications, *International Review of Electrical Engineering (I.R.E.E.)*, *vol. 9 n.* 1, January 2014, pp. 16–25.

[6] A. Trentin, P. Zanchetta, J. Clare, P. Wheeler, Automated Optimal Design of Input Filters for Direct AC / AC Matrix Converters, *IEEE Transactions on Industrial Electronics*, *vol. 59 n.* 7, July 2012, pp. 2811–2823.

[7] P. Wheeler, J. Rodríguez, J. C. Clare, L. Empringham, A. Weinstein, Matrix Converters : A Technology Review, *IEEE Transactions on Industrial Electronics*, *vol. 49 n.* 2, April 2002, pp. 276–288.
[8] M. Huang, F. Blaabjerg, P. C. Loh, The Overview of Damping Methods for Three-phase Grid-tied Inverter with LLCL-filter, *The 16th European Conference on Power Electronics and Applications, EPE'14 ECCE Europe*, August 26-28, 2014, Lappeenranda, Finlande.
[9] Y. Zhang, M. Xue, M. Li, Y. Kang, J. M. Guerrero, Co-design of the LCL Filter and Control for Grid-Connected Inverters, *Journal of Power Electronics*, *vol. 14 n.* 5, September 2014, pp. 1047–1056.
[10] J. Dannehl, M. Liserre, F. W. Fuchs, Filter-Based Active Damping of Voltage Source Converters With LCL Filter, *IEEE Transactions on Industrial Electronics*, *vol. 58 n.* 8, August 2011, pp. 3623–3633.
[11] F. A. Gervasio, R. A. Mastromauro, D. Ricchiuto, M. Liserre, Dynamic Analysis of Active Damping Methods for LCL-filter-based grid converters, *The 39th Annual Conference of the IEEE Industrial Electronics Society, IECON 2013*, November 10-13, 2013, Vienna, Austria.
[12] S. G. Parker, B. P. McGrath, D. G. Holmes, Regions of Active Damping Control for LCL Filters, *IEEE Transactions on Industry Applications*, *vol. 50 n.* 1, January 2014, pp. 424–432.
[13] D. Pan, X. Ruan, C. Bao, W. Li, X. Wang, Capacitor-Current-Feedback Active Damping With Reduced Computation Delay for Improving Robustness of LCL-Type Grid-Connected Inverter, *IEEE Transactions on Power Electronics*, *vol. 29 n.* 7, July 2014, pp. 3414–3427.
[14] S. Tang, L. Peng, Y. Kang, Active Damping Method Using Grid-Side Current Feedback for Active Power Filters with LCL Filters, *Journal of Power Electronics*, *vol. 11 n.* 3, May 2011, pp. 311–318.
[15] Z. Wan, J. Xiong, J. Lei, C. Chen, K. Zhang, A Modified Capacitor Current Feedback Active Damping Approach for Grid Connected Converters with an LCL Filter, *Journal of Power Electronics*, *vol. 15 n.* 5, September 2015, pp. 1286–1294.
[16] M. Routimo, H. Tuusa, LCL Type Supply Filter for Active Power Filter - Comparison of an Active and a Passive Method for Resonance Damping, *The 38th IEEE Annual Power Electronics Specialists Conference, PESC 2007*, June 17-19, 2007, Orlando, USA.
[17] J. He, Y. W. Li, Generalized Closed-Loop Control Schemes with Embedded Virtual Impedances for Voltage Source Converters with LC or LCL Filters, *IEEE Transactions on Power Electronics*, *vol. 27 n.* 4, April 2012, pp. 1850–1861.
[18] R. Peña-alzola, M. Liserre, F. Blaabjerg, R. Sebastián, J. Dannehl, F. W. Fuchs, Systematic Design of the Lead-Lag Network Method for Active Damping in LCL-Filter Based Three Phase Converters, *IEEE Transactions on Industrial Informatics*, *vol. 10 n.* 1, February 2014, pp. 43–52.
[19] M. Liserre, F. Blaabjerg, S. Hansen, Design and control of an LCL-filter-based three-phase active rectifier, *IEEE Transactions on Industry Applications*, *vol. 41 n.* 5, September 2005, pp. 1281–1291.
[20] H. She, H. Lin, X. Wang, L. Yue, Damped input filter design of matrix converter, *The 8th International Conference on Power Electronics and Drive Systems, PEDS 2009*, November 2-5, 2009, Taipei, Taiwan.
[21] R. Peña-Alzola, M. Liserre, F. Blaabjerg, R. Sebastían, J. Dannehl, F. W. Fuchs, Analysis of the Passive Damping Losses in LCL-Filter-Based Grid Converters, *IEEE Transactions on Power Electronics*, *vol. 28 n.* 6, June 2013, pp. 2642–2646.
[22] S. F. Pinto, J. F. Silva, Sliding mode direct control of matrix converters, *IET Electric Power Applications*, *vol. 1 n.* 3, May 2007, pp. 439–448.
[23] M. Rachid, *Power Electronics Handbook, third edition* (Elsevier Inc., 2011).
[24] C. Wessels, J. Dannehl, F. W. Fuchs, Active damping of LCL-filter resonance based on virtual resistor for PWM rectifiers – stability analysis with different filter parameters, *The 39th IEEE Annual Power Electronics Specialists Conference, PESC 2008*, June 15-19, 2008, Rhodes, Greece.
[25] F. Bronchart, Y. Mollet, J. Gyselinck, LCL Filters for a grid emulator application - Comparative study of active damping techniques, *The 39th Annual Conference of the IEEE Industrial Electronics Society, IECON 2013*, November 10-13, 2013, Vienna, Austria.
[26] A. Williams, F. Taylors, *Electronic filter design handbook* (McGraw-Hill, 2006).
[27] S. F. Pinto, J. F. Silva, Constant-frequency sliding-mode and pi linear controllers for power rectifiers: a comparison, *IEEE Transactions on Industrial Electronics*, *vol. 46 n.* 1, February 1999, pp. 39–51.

Authors' information

[1]Department of Bio, Electro and Mechanical Systems (BEAMS), Energy Group, École polytechnique de Bruxelles, Université Libre de Bruxelles, Brussels, Belgium.
[2]INESC-ID, Energy Systems, Power Electronics and Power Quality group, Instituto Superior Técnico, University of Lisbon, Lisbon, Portugal.

T. Geury was born in Brussels, Belgium in 1989. He graduated in Electrical Engineering in 2012, at Université Libre de Bruxelles (ULB). He is currently pursuing his PhD in co-supervision between the ULB, Belgium, in the BEAMS Energy research center, and the Instituto Superior Técnico (IST), Portugal, in the INESC-ID Power Electronics and Power Quality group, with a F.R.I.A. grant.
His main research interests are power electronics in PV systems and its applications and enhanced Power Quality functionalities.
Mr. Geury is a Student Member of the IEEE society.

S. Pinto was born in Coimbra, Portugal in 1969. She graduated in Electrical Engineering in 1995 and received the Doctor in Electrical and Computer Engineering Degree in 2003, from Instituto Superior Técnico (IST), University of Lisbon, Portugal. Currently, she is an Assistant Professor of Power Electronics at the same University and a member of the INESC-ID Power Electronics and Power Quality group.
Her main research interests are Power Electronic Systems modeling, simulation and advanced control and Power Quality enhancement applications and evaluation.
Prof. Pinto is a Senior Member of the IEEE society.

J. Gyselinck was born in Ghent, Belgium in 1967. He graduated in electrical and mechanical engineering in 1991 and received the Doctor of Applied Sciences degree in 2000, both from the Ghent University, Belgium. From 1993 till 2000 he was Research Assistant with the Electrical Energy Lab (EELAB) of the Ghent University. From 2000 till 2004 he was researcher and lecturer with the Department of Electrical Engineering of the University of Liège, Belgium. He is currently a professor at École polytechnique de Bruxelles (EPB), Université Libre de Bruxelles (ULB), teaching courses on electrical machines and power electronics, and a member of the BEAMS Energy research group.
His past and present research mainly concerns the numerical computation of magnetic fields (mostly using the finite element method) and the simulation of electrical machines.
Prof. Gyselinck is a Member of the IEEE society.